Available online at www.sciencedirect.com
SCIENCE DIRECT
Polymer 47 (2006) 3207–3217
polymer
www.elsevier.com/locate/polymer

A study on the photo-degradation of zinc oxide (ZnO) filled polypropylene nanocomposites

Hongxia Zhao, Robert K.Y. Li *

Department of Physics and Materials Science, City University of Hong Kong, Tat Chee Avenue, Kowloon, Hong Kong, China

Received 9 September 2005; received in revised form 21 February 2006; accepted 28 February 2006
Available online 23 March 2006

Abstract

This research aims to study the photo-degradation characteristics for zinc oxide (ZnO) nanoparticle filled polypropylene (PP) nanocomposites. By paying attention to the evolution of the carbonyl absorption bands from FTIR analysis, it has been observed that UV irradiation induced significant photo-degradation for unfilled PP. However, with the incorporation of ZnO nanoparticles into the PP matrix, the extent of photo-degradation was significantly reduced. This is due to the superior UV light screening effects offered by the ZnO nanoparticles. WAXD measurements showed that β-form PP crystal had been induced in the PP/ZnO nanocomposites. An interesting observation from this study is that β-form PP crystal was also induced in unfilled PP due to UV irradiation. UV-irradiation induced degradation caused a significant drop in the ductility for unfilled PP. With the incorporation of ZnO nanoparticles, the ductility, and hence the tensile strength were recovered to some extent. The higher the ZnO particle content, the higher the elongation at break value in the UV irradiation treated nanocomposites. It was also observed that surface cracks were induced by photo-degradation, and the Talysurf surface profile measurements indicate that the severity of the surface cracks were significantly reduced in the ZnO/PP nanocomposites.

Keywords: Zinc oxide nanoparticle; Photo-degradation; Nanocomposite

1. Introduction

Degradation of polymeric materials is a commonly encountered phenomenon that leads to changes in their chemical, physical, and mechanical properties. There are many factors causing polymer degradation: solar light or other high energy radiations, heating, chemicals attack, stress loading, water absorption, biological sources, and so forth [1]. Among these factors, ultraviolet (UV) irradiation is a frequently encountered factor that can induce photo-degradation of polymers under outdoor service environments.

Polypropylene (PP) is one of the most extensively used polyolefins, and with a significant portion of its applications being under outdoor environments. Its exposure to sunlight and the related degradations are important issues that have attracted active research interest. Severe molecular chain degradation in PP can be induced when it is irradiated within the active wavelength range of 310–350 nm [1], which means that photo-degradation can occur easily in PP based materials. A number of reviews and research articles have been dedicated to the mechanisms of UV-induced degradations in PP [2–9].

With their rapid developments, there is a growing interest in understanding the thermal stability and degradation behavior of polymeric nanocomposites. A good knowledge on these issues will be critical for assessing the service lifetime for components fabricated using nanocomposites. There are a number of recent studies on the thermal stability, thermal degradation kinetics and mechanisms, and photo-degradation for nanocomposites [10–19]. It is interesting to note that the majority of these studies are concerning with montmorillonite (MMT) based nanocomposites. In the study by Qin et al. [14], it was observed that by introducing MMT particles into LDPE matrix, the rate of photo-oxidative degradation was much faster than pure HDPE. Furthermore, the dispersion state of the MMT particles did not seem to have influence on the photo-degradation rate. In subsequent studies on MMT filled PP nanocomposites, Qin et al. [15] and Morlat et al. [16] further observed the detrimental influence of MMT particles on the photo-degradation rate of the PP matrix.

In the majority of studies on the photo-degradation of PP or its nanocomposites, the main focuses were on the degradation

* Corresponding author. Tel.: +852 2788 7785; fax: +852 2788 7830.
E-mail address: aprkyl@cityu.edu.hk (R.K.Y. Li).

0032-3861/$ - see front matter © 2006 Elsevier Ltd. All rights reserved.
doi:10.1016/j.polymer.2006.02.089

mechanisms and degradation rates, and the resulting changes in the mechanical properties were rarely addressed. It is well known that the most significant consequence of UV irradiation is the embrittlement effect to the polymer, and in particular, to their surfaces. Usually surface cracks are formed due to contraction of the surface layer, which is the main cause for the serious deterioration in mechanical properties (especially the ductility) of photodegraded products [20]. Therefore, an understanding on the effect of UV light on the mechanical properties is necessary for a better understanding on the performance of nanocomposites.

In terms of UV irradiation damage, a number of researches are of particular interest. It has been reported that zinc oxide (ZnO) particle and ZnO doped ceramic particle are effective UV light screen material [9,21]. Moustaghfir et al. [22] reported results of accelerated UV irradiation test on zinc oxide sputter coated polycarbonate (PC) films. The main conclusion was that the rate of oxidation and the subsequent photo-degradation of PC was reduced, which were due to the screening effect of the coating and the lowered oxygen diffusion rate. It would thus be of interest to develop nano-size ZnO filled polymer nanocomposites for engineering applications. Thus, the main objectives of this research are to develop and characterize ZnO nanoparticle filled PP nanocomposites. In particular, the effectiveness of ZnO nanoparticles on combating UV irradiation damage for PP will be evaluated.

2. Experimental

2.1. Materials and ZnO/PP nanocomposite preparation

The zinc oxide (ZnO) nanoparticles (Nano Tek® Zinc Oxide C1) used in this work were supplied by Nanophase Technology Co. They were surface treated with an organo-silane coupling agent in the supplied form. A commercial grade of polypropylene (Pro-fax 6331) was used as the matrix. The ZnO nanoparticles and PP pellets were melt-mixed in a Brabender twin screw extruder. The ZnO nanoparticle content in the composites are 1.5, 3.0, and 5.0 wt%, respectively. For comparative purpose, samples of unfilled PP were also subjected to the same blending procedure so that unfilled PP and the PP matrix for the nanocomposites had experienced similar processing histories. The melt-blended extrudates were then injection molded into plates with dimensions of 200×80×3 mm. For PP containing 0, 1.5, 3.0, and 5.0 wt% of ZnO nanoparticles, the materials will be designated as PP, ZnO-1.5, ZnO-3.0, and ZnO-5.0, respectively. For the material systems subjected to UV-irradiation treatment (details to be given below), they will be referred to as UV-PP, UV-ZnO-1.5, UV-ZnO-3.0, and UV-ZnO-5.0, respectively.

2.2. Characterizations and measurements

UV irradiation treatment for unfilled PP and the ZnO/PP nanocomposites were carried out using a QUV accelerated weathering tester (Q-panel lab products, UVA 340 nm), with a light intensity of 0.65 W/m^2. The two surfaces of the injection molded plates were each subjected to the UV irradiation treatment for 300 h, hence the total exposure time for each plate was 600 h. During irradiation treatment, the working temperature was controlled at 65 °C. After UV irradiation treatment, the samples were subjected to Fourier transformed infrared (FTIR) analysis. Samples of about 0.5 mm thick were cut from the surface of the plates and powdered. Subsequently, the powders were mixed and cold pressed with KBr to produce disks [11,23]. FTIR measurement (model 16PC, Perkin–Elmer) was carried out at transmission mode using 20 scans at 2 cm^{-1} resolution. KBr was used as the spectrum background. PP molecular degradation was characterized by the carbonyl index, which was calculated by Eq. (1):

$$\text{Carbonyl index} = \frac{A_C}{A_R} \tag{1}$$

In Eq. (1), A_C is the area of the carbonyl absorption band (in the range from 1700 to 1800 cm^{-1}), and A_R is the area of the reference band (in the range from 2700 to 2750 cm^{-1}). The carbonyl band reflects several degradation products. The reference band will not be affected by either photo-oxidation nor by varying crystallinity [5,23].

Differential scanning calorimetry characterization (model DSC 2910, TA Instruments) was performed to investigate the crystallization and the melting behaviors of the nanocomposites. Thin slices of samples about 0.5 mm thick were cut from the surfaces of the molded plates for the measurement. The heating (and cooling) rate used was 10 °C/min for both heating and cooling scans. The crystallinity for unfilled PP and the PP matrix of the ZnO/PP nanocomposites were calculated according to the DSC data from the heating scan. The enthalpy of fusion (ΔH_f), enthalpy of crystallization (ΔH_c), temperature of melting and crystallization (T_m and T_c), and crystallinity (X_c) of PP for the different nanocomposites were measured. The enthalpy of melting for 100% crystalline PP was taken to be $\Delta H_m^0 = 209$ J/g[24].

The crystal structure of the ZnO/PP nanocomposites were studied by wide angle X-ray diffraction (WAXD) measurement. It was conducted by using a Philips X'Pert diffractometer with Cu Kα radiation ($\lambda = 1.542$ Å). The scanning rate used was 0.02°/min and the scanning angle was from 5 to 35°. WAXD measurements were carried out on both skin and core regions of the molded plates. For measurements to the core region, the molded plates were sectioned along the mid-plane.

2.3. Mechanical property tests

Dynamic mechanical analysis (DMA 2980, TA Instruments) was performed to obtain the storage and loss moduli of the nanocomposites before and after UV irradiation treatment. The dual cantilever mode was used for the test, with the oscillation amplitude and frequency being 10 μm and 1 Hz, respectively. DMA specimens were cut with the long dimension of the specimen parallel to the long dimension of the molded plates.

Tensile stress–strain curves were measured using an Instron 5507 testing machine. The cross-head speed and test temperature were 5 mm/min and 23 °C, respectively.

2.4. Microscopic observation and surface profile measurement

The ZnO nanoparticles and their dispersion in PP matrix were observed by using a transmission electron microscope (TEM, Philips CM20). Scanning electron microscopy (SEM, Jeol JSM 6335F) was used to observe the fracture surfaces after tensile tests. Surface cracking patterns for the UV irradiation treated samples were observed by using an optical microscope (OM, Olympus BH2). The profiles of these surface cracks were measured by using a Form Talysurf PGI surface texture tester. The scanning rate was 0.5 mm/s.

2.5. Thermal stability analysis

Thermal stability of specimens before and after UV irradiation was characterized by using a thermogravimetric analyzer (TGA, SII, SSC/5200 H, Seiko Instruments). The system can be operated in the simultaneous TGA/DTA mode. Measurements were conducted under a helium flow rate of 300 mL/min at a heating rate of 20 °C/min. The scanning temperature was from 25 to 500 °C. Similar to the DSC characterizations, thin slices of samples about 0.5 mm thick were cut from the surfaces of the molded plates for the measurement.

3. Results and discussions

3.1. Dispersion of nanoparticles in PP matrix

Fig. 1 is the TEM image for the as-received ZnO nanoparticles. It can be observed that most of the nanoparticles are in nano-meter scale and are mostly of elongated shape. In addition, some irregular shaped ZnO particles can also be found. The dispersion state of the nanoparticles in ZnO-3.0 (i.e. the composite that contained 3.0 wt% of ZnO nanoparticles) is shown in Fig. 2. As can be seen, most of the nanoparticles are uniformly dispersed in the PP matrix. It has been established that the organic nature of nanoparticle surfaces is a key factor

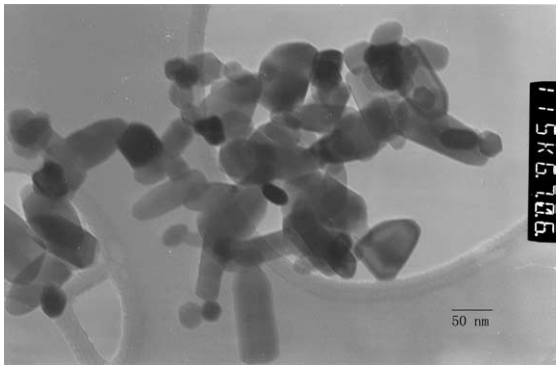

Fig. 1. TEM image for the as received ZnO nanoparticles.

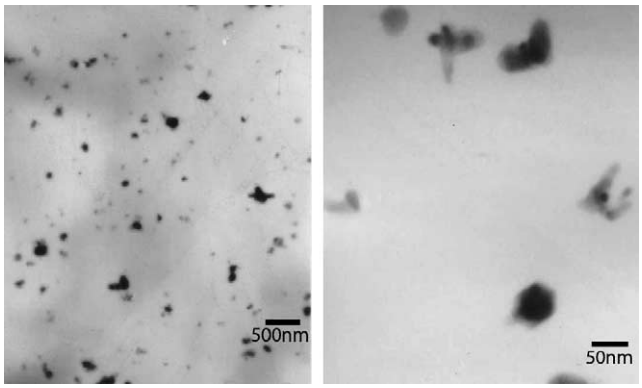

Fig. 2. TEM images for the ZnO-3.0 nanocomposite at different magnifications.

to promote the dispersion of the nanoparticles in the matrix [25,26]. Therefore, the presence of the organic surface treatment on the ZnO particles, which changes the surface properties from inorganic into organic, reduces the particle surface tension. This is essential to promote the uniform dispersion of the ZnO nanoparticles in the PP matrix.

3.2. FTIR analysis

Generally speaking, photo-oxidation processes belong to radical reactions, which are initiated mainly by two sources: (1) high energy photon collision; and (2) the presence of impurities such as trace metals left from the polymerization processes [1]. The consequence of photo-oxidation of PP is the formation of hydroperoxides and carbonyl species such as ketones, esters, and acids [15,16]. By using FTIR spectroscopy, the degradation products will induce the evolution of absorption peaks in the wavenumber ranges of 3200–3600 and 1600–1800 cm^{-1}, respectively. For a qualitative description of the extent of photo-oxidation in this research, the evolutions of the FTIR spectrum in the wavenumber range of 1600–1800 cm^{-1} were examined. The FTIR results for the UV irradiation treated ZnO/PP nanocomposites are presented in Fig. 3. For

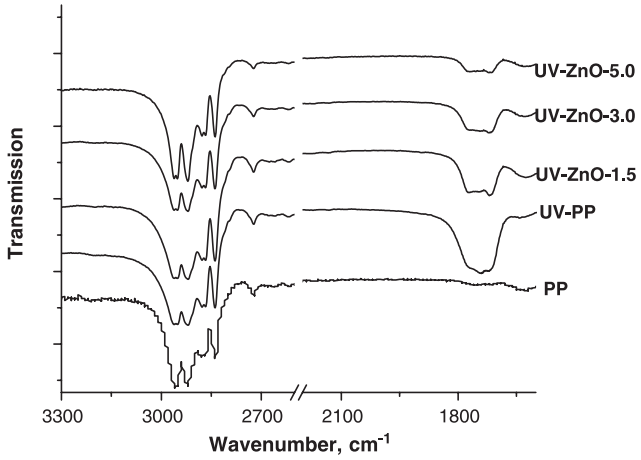

Fig. 3. FTIR spectrum for unfilled PP and ZnO/PP nanocomposites after UV irradiation treatment. The spectrum for unfilled PP before irradiation is also shown.

comparative purpose, the spectrum labeled PP (i.e. unfilled PP sample before UV irradiation) was also shown. Additionally, the characteristic peaks for PP (in the wavenumber range of 2800–3000 cm^{-1}, which are related to the asymmetric and symmetric C–H stretching vibration [27]) are also included in Fig. 3 for the respective samples. By comparing the evolution of the absorption peaks within the carbonyl region (i.e. 1700–1800 cm^{-1}) to the characteristic peaks for PP in the wavenumber range of 2800–3000 cm^{-1}, a rough estimate to the extend of photo-degradation can be obtained [27,28]. On comparing the spectrum for PP and UV-PP, the evolution of the absorption peaks within the carbonyl region is very dramatic. The evolution of the characteristic peaks for the photo-degradation of PP has been studied in detail [29]. It has been documented that at the beginning of the UV exposure period, carboxylic acid was initially formed (absorption bands centered at 1712 cm^{-1}). With exposure periods longer than 60 h, absorption bands at 1720 and 1780 cm^{-1} was starting to form, and this indicates the formation of ketones and lactones [5].

In addition, for a more quantitative expression for the extent of the photo-degradation, the carbonyl index (Eq. (1)) for PP as a function of ZnO nanoparticle content after UV-irradiation treatment is shown in Fig. 4. The striking observation from both Figs. 3 and 4 is that for the nanocomposites with increasing ZnO particle content, the peak intensities decreased correspondingly. It thus can be deduced that ZnO nanoparticles play an important role in stabilizing the PP molecules and delay the photo-degradation process by acting as screens. The dominant screening mechanism is that the ZnO nanoparticles absorbed the UV radiation and hence reduced the UV intensity that can promote the oxidation of the PP chains. However, as no new peaks were observed after UV irradiation in the ZnO/PP nanocomposites when compared to UV-PP, the photo-degradation mechanisms for PP and ZnO/PP nanocomposites should be identical. The mechanisms of photo-degradation include the formation of carboxylic acids and other carbonylated products generated by macroradical oxidation [9,30,31]. Similar outstanding photo-stabilization effect of ZnO nanoparticles on LLDPE has also been reported by Yang el al [19]. It is also worth to note that for the photo-oxidation of MMT/PP nanocomposites, while the rate of PP oxidation was significantly modified by the MMT nano-layers, the mechanisms of photo-degradation were also observed to be unmodified [15,16].

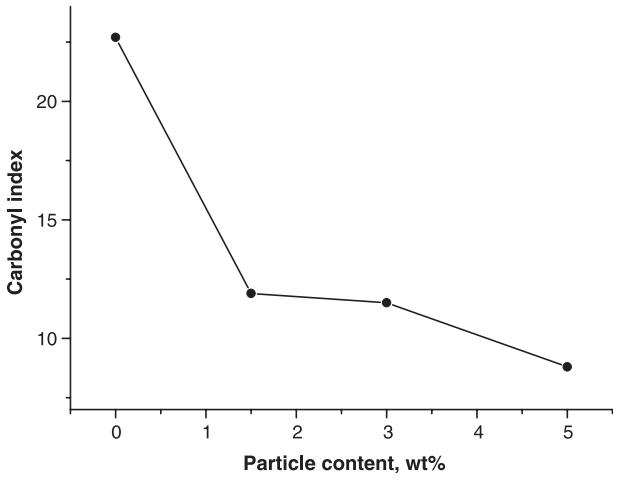

Fig. 4. Effect of ZnO nanoparticle content on the carbonyl index for the UV irradiation treated nanocomposites.

3.3. Effect of UV irradiation on thermal and crystallization behaviors

3.3.1. DSC results

DSC data for unfilled PP and ZnO/PP nanocomposites before UV irradiation are summarized in Table 1. The melting behavior of PP, as reflected by both ΔH_f and $T_{m,}$ was not affected by increasing ZnO nanoparticle content. However, the crystallization temperature tends to shift to higher values with increasing ZnO nanoparticle content. This implies that the existence of ZnO nanoparticles facilitates the crystallization of PP and this effect becomes more evident with higher nanoparticle content. Tang et al. [32] has also observed that after the incorporation of 2 wt% of ZnO nanoparticles, the crystallization temperature of PP was increased from 111 to 114 °C. Furthermore, micron-size ZnO has similar effect on PP's crystallization temperature in comparison to ZnO nanoparticles. From Table 1, it can also be seen that the crystallinity (X_c) increases slightly by the incorporation of ZnO nanoparticles, from 38.7% for PP to 41.1% for the ZnO-5.0 nanocomposite. It is generally expected that nanofillers will act as nucleating agents in polymer crystallization. However, experimental observations showed diversified results [33–35]. For nano $CaCO_3$ filled PP, the observation was that increasing nanofiller content did not affect the PP crystallinity (which remained at around 51%) [35]. However, for clay/PP nanocomposites, there are contradictory observations on crystallization studies—either increase [33] or decrease [34] in PP crystallinity due to the addition of MMT have been reported.

By comparing the data in Tables 1 and 2, it can be seen that UV irradiation treatment has obvious influence on both the crystallization and melting behaviors of the PP matrix. The melting temperature (T_m) of unfilled PP dropped from 168.6 to 163.8 °C. In comparison, the reduction in T_m for the ZnO/PP nanocomposites due to UV irradiation is relatively insignificant. Besides, it can be noted that X_c increases significantly for the unfilled PP upon UV irradiation (from 38.7 to 46.4%), while X_c for the ZnO/PP nanocomposites are not much affected by UV irradiation. When a semi-crystalline polymer is exposed to UV irradiation, chemi-crystallization will take place [20]. There are reports that the crystallinity of PP increases with increasing UV exposure time, especially at the early exposure stage [5,8]. It is well known that chain scission caused by photo-degradation can release the entanglement of molecules and produce more freed segments. As a result, more segments can move into the original crystals or form new crystalline structure in the original amorphous zone, especially at an elevated exposure temperature (65 °C in our case). The insignificant variation in X_c for the ZnO/PP nanocomposites

Table 1
Thermal and crystallization data obtained from DSC and DMA for the nanocomposites before UV irradiation treatment

	ΔH_f (J/g)	T_m (°C)	ΔH_c (J/g)	T_c (°C)	X_c (%)	T_g by DMA (°C)
PP	80.95	168.6	97.25	110.8	38.7	9.1
ZnO-1.5	79.76	168.7	94.81	112.1	38.7	8.9
ZnO-3.0	80.91	168.2	95.65	113.0	39.9	8.5
ZnO-5.0	82.13	168.9	96.14	113.8	41.1	7.9

Table 2
Thermal and crystallization data obtained from DSC and DMA for the nanocomposites after UV irradiation treatment

	ΔH_f (J/g)	T_m (°C)	ΔH_c (J/g)	T_c (°C)	X_c (%)	T_g by DMA (°C)
UV-PP	97.03	163.8	90.83	109.5	46.4	8.5
UV-ZnO-1.5	86.30	167.2	93.97	111.8	41.9	10.1
UV-ZnO-3.0	81.44	167.1	90.09	111.9	40.2	10.4
UV-ZnO-5.0	78.77	166.8	90.08	112.1	39.7	11.2

may be due to one or both of the following factors: (i) the extent of photo-degradation of the ZnO/PP nanocomposites is lower than that of the virgin PP; and (ii) there is a stabilization function of the ZnO nanoparticles in blocking the chemi-crystallization of PP.

3.3.2. WAXD results

The commonly found crystalline forms in bulk PP are the monoclinic α and hexagonal β forms. With these two crystalline forms, α crystal is the most commonly occurring crystal structure in PP and β crystal only forms under special conditions such as quenching or using specific nucleating agents [36]. Fig. 5(a) shows the WAXD curves for PP, ZnO nanoparticle and the ZnO-3.0 nanocomposite (taken before UV irradiation treatment). It is evident that the two prominent peaks existing at $2\theta > 30°$ are the characteristic peaks for ZnO, while the diffraction peaks for PP occur at $2\theta < 30°$ [36,37]. For PP without subjected to UV irradiation treatment (the diffractogram labeled PP in Fig. 5(a)), only α crystals can be found. However, for the ZnO-3.0 nanocomposite, a small peak can be observed at $2\theta = 16.2°$, indicating the presence of β crystal form. It can be induced that the β form PP crystals were induced by the introduction of ZnO-nanoparticles. The ZnO-nanoparticles acted as nucleating agent to develop a small amount of β crystals. Other inorganic nanoparticles, such as $CaCO_3$ [35] and Al_2O_3 [38], have been observed to nucleate β crystals in PP matrix.

The WAXD curves for UV-PP and the UV-ZnO-3.0 nanocomposite (i.e. after UV irradiation) are shown in Fig. 5(b). Measurements had been carried out on the skin and core regions separately and the results are compared. For the UV-PP sample taken from the skin (labeled UV-PP-skin), a pronounced new peak due to the presence of β-PP crystal was formed. This β-peak was absent in the PP sample before UV treatment (see the curve labeled PP in Fig. 5(a)). This gives evidence that UV-irradiation can induce the formation of β-PP crystals. As one moved toward the core (the curve labeled UV-PP-core in Fig. 5(b)), it can be seen that the amount of β crystals was reduced significantly when compared to the UV-PP-skin sample. This is reasonable due to the limited UV light penetration and the deficiency of oxygen molecules in the core of the specimen. As a result, the extent of chemi-crystallization is more pronounced in the surface (skin) layer than the core region.

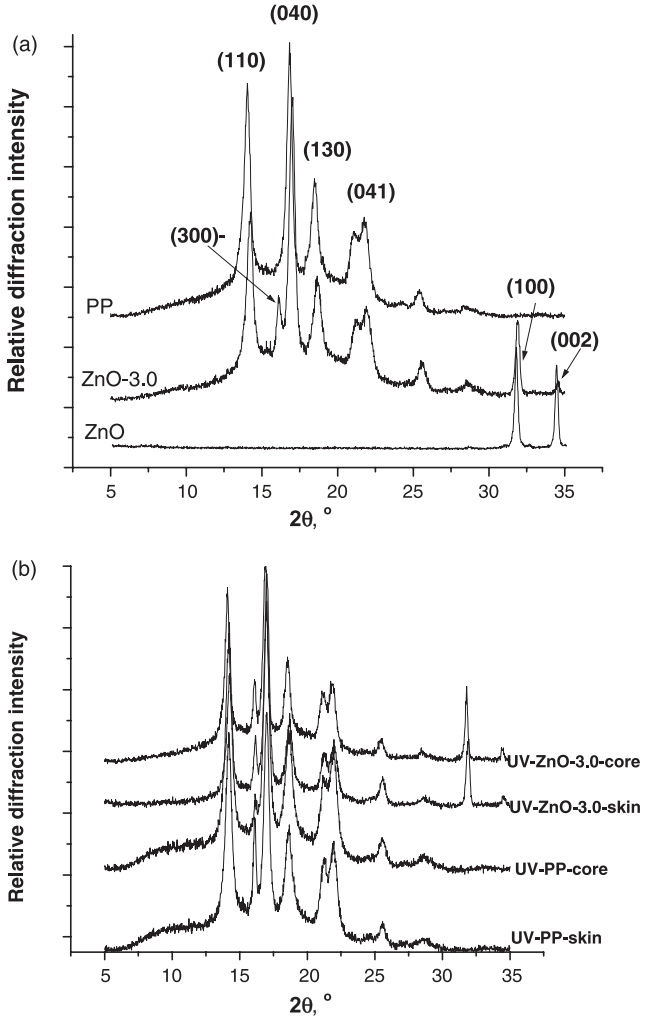

Fig. 5. WAXD curves for unfilled PP, ZnO nanoparticle, and ZnO/PP nanocomposite containing 3.0 wt% of nanoparticles: (a) before UV irradiation treatment; and (b) after UV irradiation treatment.

For the UV-ZnO-3.0 nanocomposite (Fig. 5(b)), there is no significant difference in the intensities of the β crystal diffraction peak for the skin (UV-ZnO-3.0-skin) and core (UV-ZnO-3.0-core) regions. This can be reasoned by the strong UV absorption capability of the ZnO nanoparticles. Hence, the secondary chemi-crystallization caused by UV photo-degradation to form the β-PP crystals in the skin was suppressed.

The presence of β-PP crystals is known to have influences on the mechanical response of polypropylene, in particular, the improvement in impact strength [39–42]. Karger-Kocsis and Varga [43] have also reported noticeable improvement in the work of fracture for β-PP under quasi-static loading rate. It has been postulated that one of the possible toughening mechanisms of β-PP is the βα-transformation. The βα-transformation has been observed to depend on the local deformation of the strain field as well as the loading rate. The photo-degradation of β-PP has been studied by Kotek et al. [4] and Obadal et al. [5]. In comparison to the corresponding α-PP, β-PP has significantly better resistance to photo-degradation in terms of the formation of degradation by products (expressed by the carbonyl index) [5] and residual mechanical properties [4]. In the current study, the presence of a small fraction of β-PP crystals in the original (i.e. before UV-irradiation treatment) ZnO/PP nanocomposites may has beneficial effect to reduce photo-degradation. Further works are needed in order to understand the presence/absence of any synergistic effects due to the co-existence of β-PP crystals and ZnO nanoparticles on PP photo-degradation.

3.4. Effect of UV irradiation on mechanical properties

3.4.1. DMA results

Fig. 6 presents the dynamic mechanical properties of the ZnO/PP nanocomposites before and after UV irradiation treatment. It can be observed that under a given treatment condition (i.e. before or after UV irradiation treatment), the storage modulus (E') increases with increasing nanoparticle content (Fig. 6(a)). This is expected owing to the stiffness improvement effect of inorganic ceramic particles. On comparing the storage modulus curves for PP and UV-PP samples, it can be seen that E' at −50 °C was reduced dramatically from about 4600 MPa for PP to 2700 MPa for UV-PP. In contrast, the corresponding reduction in E' due to UV irradiation treatment for the ZnO/PP nanocomposites is less significant as the ZnO content increases. This shows that the ZnO/PP nanocomposites have better ability to maintain their stiffness even after photo-degradation.

The loss modulus (E'') vs. temperature plots for the different materials systems are shown in Fig. 6(b), with the plots being shifted vertically for easy identification. The glass transition temperature (T_g) for the PP phase in the different material systems before and after UV irradiation treatment are summarized in Tables 2 and 3, respectively. As can be seen from Table 2, before UV irradiation treatment, the addition of ZnO nanoparticles does not have any obvious effect on the T_g of PP. For PP subjected to UV irradiation treatment, the photo-degradation will cause both chain scission and chain cross-linking [6], which will induce different effects on the molecular chain motions. On the one hand, chain scission generates more free short chains that move more easily and hence render a lower T_g. On the other hand, cross-linking increases T_g by restricting the movement of molecules. T_g for the UV irradiation treated virgin PP is then controlled by these two competing factors, with the end result that no obvious change could be observed. For the ZnO/PP nanocomposites, the situation becomes much more complicated owing to the addition of nanoparticles. Based on Fig. 6(b) and Table 3, T_g for the nanocomposites were increased after UV irradiation. This can be explained as follows: ZnO nanoparticles can serve

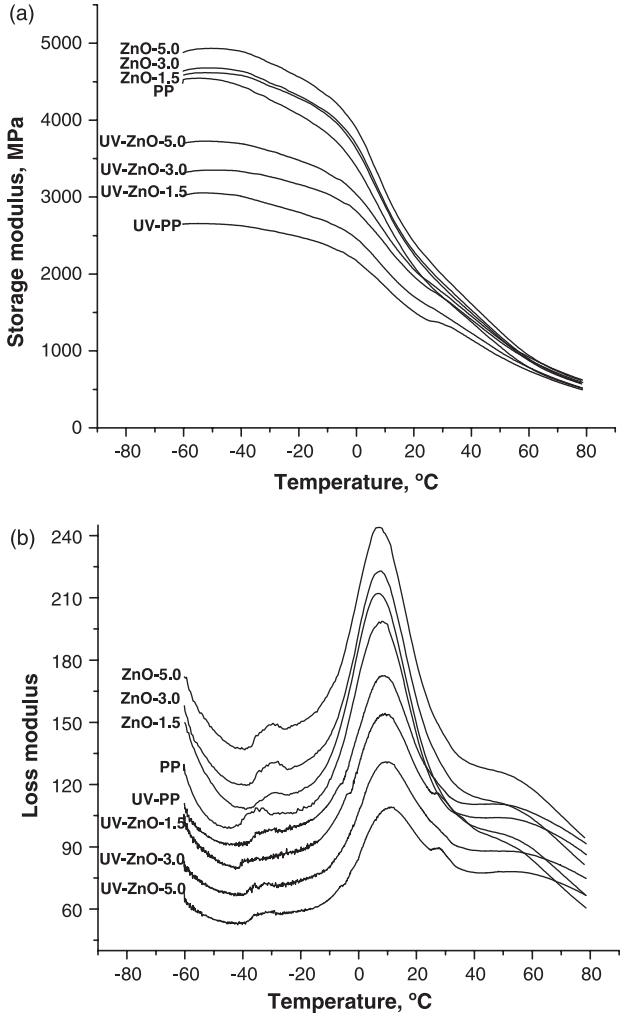

Fig. 6. Dynamic mechanical analysis of unfilled PP and ZnO/PP nanocomposites: (a) storage modulus vs. temperature plots; and (b) loss modulus vs. temperature plots.

Table 3
3 $T_{-5\%}$ and T_{max} measured by TGA

	$T_{-5\%}$ (°C)	T_{max} (°C)
PP	405.1	465.5
UV-PP	335.0	462.6
UV-ZnO-1.5	408.4	471.1
UV-ZnO-3.0	417.2	475.0
UV-ZnO-5.0	412.8	477.6

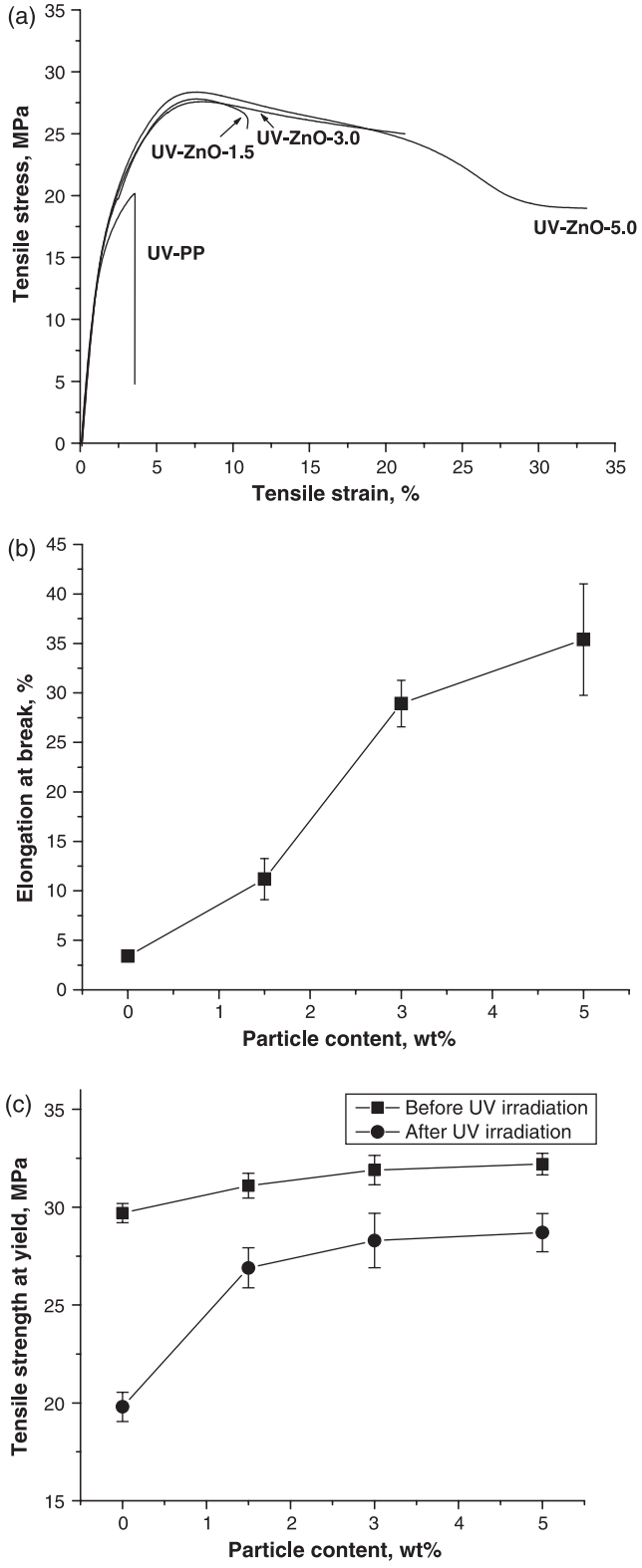

Fig. 7. Tensile characteristics for unfilled PP and ZnO/PP nanocomposites: (a) tensile stress–strain curves after UV irradiation treatment; (b) elongation at break for unfilled PP and ZnO/PP nanocomposites after UV irradiation treatment; and (c) effect of UV irradiation treatment on the tensile strength at yield for the nanocomposites.

as physical cross-linking points to anchor the PP molecular chains to certain extent. Before UV irradiation, the PP chains are severely entangled and the function of nanoparticles as physical anchorage points is relatively insignificant. The mobility of molecular chain segments is largely determined by entangling conditions. Therefore, T_g of PP does not have a clear variation by introduction of the ZnO nanoparticles. When UV irradiation treatment was introduced, the degradation makes PP molecular chains much shorter and the degree of chain entanglement drops dramatically. In this case, the function of nanoparticles as physical cross-linking points becomes pronounced. As a result, T_g increases as the content of ZnO nanoparticles is increased.

3.4.2. Tensile behaviors

Under quasi-static tensile loading and before UV irradiation treatment, virgin PP and the ZnO/PP nanocomposites showed highly ductile behavior, with all the tensile specimens having elongation at break to be over 500% of strain. However, after UV irradiation treatment, the ductility of the tensile specimens were reduced markedly. Typical stress–strain curves for UV irradiation treated virgin PP (UV-PP) and the nanocomposites are shown in Fig. 7(a). It can be seen that the UV-PP became very brittle with the elongation at break dropped to only 4%.

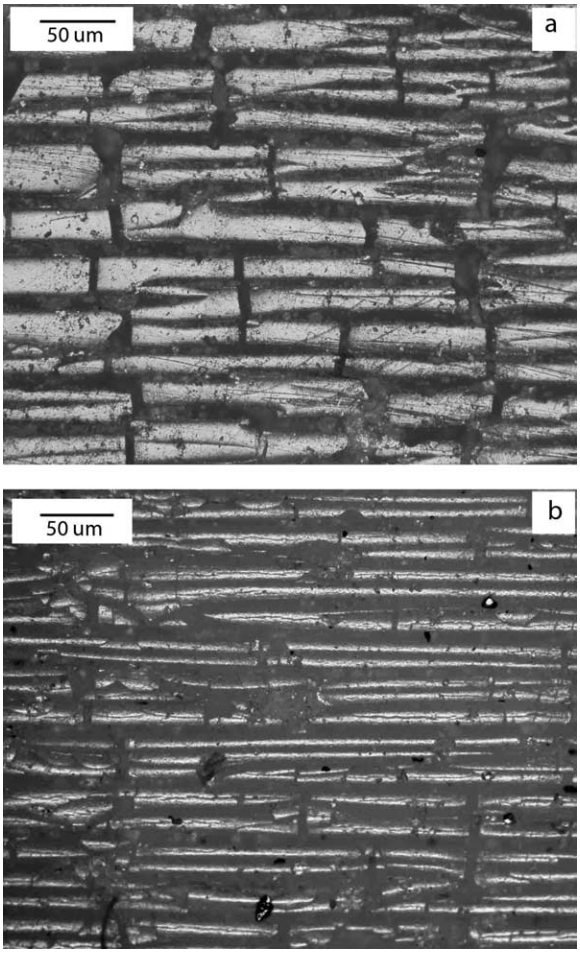

Fig. 8. Optical micrographs showing specimen surface cracks after UV irradiation treatment: (a) UV-PP; and (b) UV-ZnO-5.0.

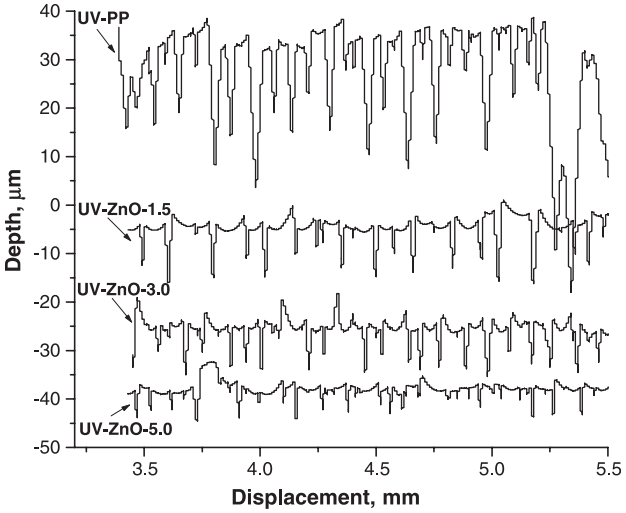

Fig. 9. Talysurf surface texture measurements showing the surface cracking profiles for unfilled PP and ZnO/PP nanocomposites after UV irradiation treatment.

The ductility for the UV irradiation treated specimens recovered to certain extent after the incorporation of ZnO nanoparticles—the higher the ZnO nanoparticle content the higher the dutility. The elongation at break for UV-PP, UV-ZnO-1.5, UV-ZnO-3.0, and UV-ZnO-5.0 are summarized in Fig. 7(b). Therefore, the resistance of PP to photo-degradation embrittlement can be improved significantly with the addition of ZnO nanoparticles.

The effect of ZnO nanoparticle content on the tensile strength at yield (σ_y) for the nanocomposites is shown in Fig. 7(c). For a given pre-treatment condition (i.e. UV-treated or non-UV-treated), the overall trend is that σ_y increases with increasing ZnO particle content. This result suggests that the interfacial interaction between the ZnO nanoparticles and the PP matrix is strong enough to delay the massive shear yielding along the tensile loading direction. For the systems with a given ZnO particle content, it is also evident from Fig. 7(c) that σ_y was reduced after UV-irradiation treatment. For unfilled PP, the UV-induced reduction in σ_y is more pronounced than that found for the ZnO/PP nanocomposites. This observation also supports the assumption that the UV-induced degradation in the ZnO nanoparticle filled PP is less severe than that in the virgin PP.

Based on the tensile test results, it can be summarized that the presence of the ZnO nanoparticles in PP matrix can act as effective UV light screen to reduce the degree of photo-degradation for the PP molecular chains.

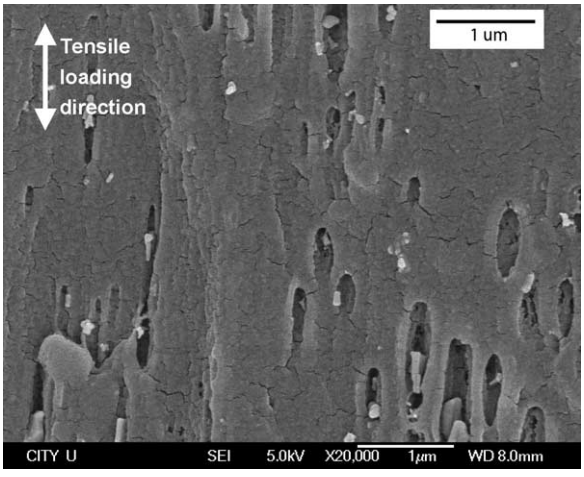

Fig. 10. SEM micrograph showing the cryo-fractured surface for the cold-drawn section of a ZnO-5.0 tensile tested specimen.

3.5. Morphological study

3.5.1. Cracking of surface layers after UV irradiation

Due to the limited penetration ability of UV light and oxygen diffusion, the degree of photo-oxidation decreases as

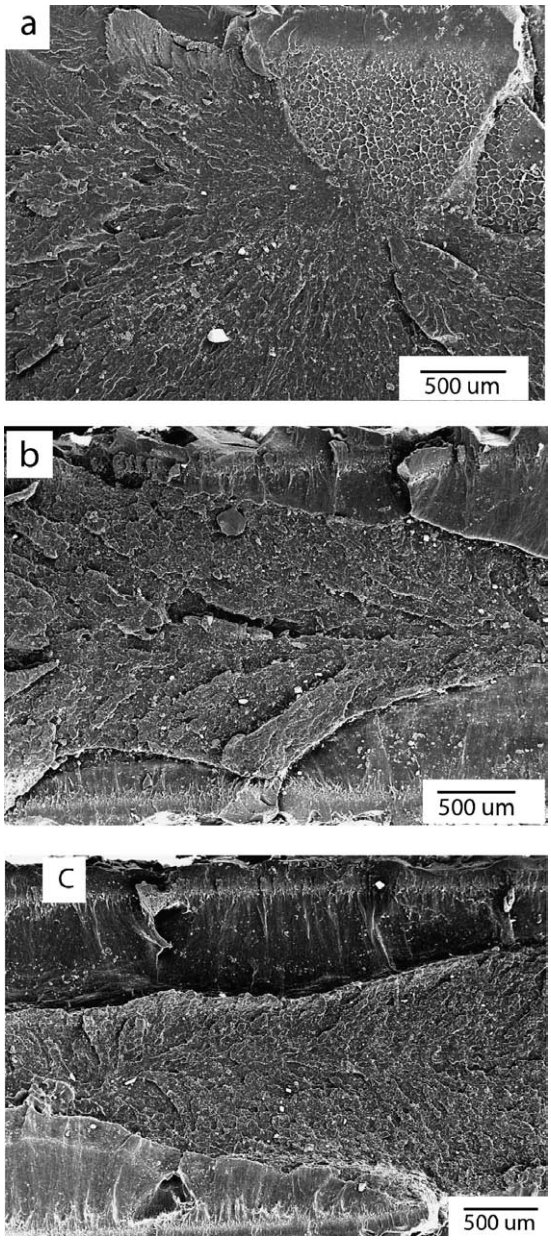

Fig. 11. Tensile fracture surfaces for unfilled PP and ZnO/PP nanocomposites after UV irradiation treatment: (a) UV-PP; (b) UV-ZnO-1.5; and (c) UV-ZnO-5.0.

one moves deeper below the material surface. Therefore, damages caused by UV irradiation and the resulting embrittlement are most serious in the surface layer and surface cracks are usually formed. Fig. 8(a) and (b) compares the surface topography for the UV-PP and UV-ZnO-5.0 nanocomposite, respectively (both photographs are optical microscopy images). For both cases, cracks caused by UV irradiation can be clearly observed. However, the cracks on the surface of UV-PP are very coarse while that for UV-ZnO-5.0 are much finer. This means that the damage caused by UV irradiation to the virgin PP is more serious than to the nanocomposite. In order to find out the cracking profiles induced by UV irradiation for the materials, surface roughness measurements were conducted and the results are shown in Fig. 9. It is obvious that the depth of the surface cracks was reduced dramatically after the addition of ZnO nanoparticles. The average crack depth was about 20 μm for UV-PP, and was reduced to only 10 μm for UV-ZnO-1.5, which corresponded to a reduction of 100%. Moreover, the crack depth was reduced further to around 5 μm for UV-ZnO-5.0. Hence, the addition of the ZnO nanoparticles can reduce the damage of UV light on PP and this effect becomes more and more evident with increasing nanoparticle content.

3.5.2. Morphologies of tensile fracture surfaces

As mentioned earlier, before UV irradiation treatment, the PP and nanocomposites exhibit high ductility under tensile loading. Fig. 10 shows the SEM image for a cryo-fractured ZnO-5.0 tensile specimen in the cold-drawn region. Due to the large differences in elastic nature between the inorganic ZnO and PP matrix, the ZnO nanoparticles act as stress concentrators and produce high tensile stress between the phases. Debonding then takes place around the ZnO nanoparticles and initiates the subsequent matrix shear yielding. Debonding can release the triaxial tensile stress and initiate the matrix deformation that followed. There are a lot of fine cracks in the PP matrix, most of which are perpendicular to the tensile loading direction and thus are probably caused by crazing of the matrix.

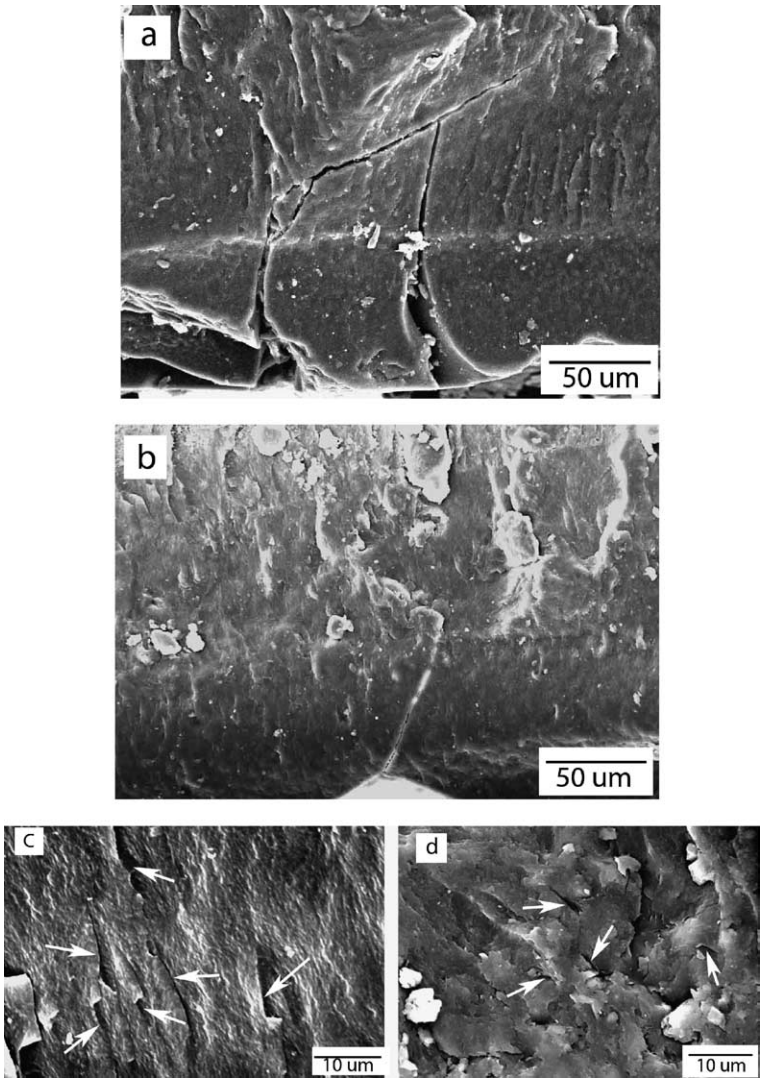

Fig. 12. SEM micrographs showing the edge zones on the tensile fracture surfaces: (a) and (c) are for UV-PP; and (b) and (d) are for UV-ZnO-3.0.

In order to investigate the effect of UV irradiation on the fracture morphology of PP and the ZnO/PP nanocomposites, SEM examination was carried out to inspect the tensile fractured surfaces. Fig. 11(a)–(c) shows the overviews of the fracture surface morphologies for the UV-PP, UV-ZnO-1.5, and UV-ZnO-5.0 tensile specimens, respectively. It is observed that the fracture surface of UV-PP is quite brittle and there is only a limited yielding zone that is confined to the upper-right region of the SEM micrograph in Fig. 11(a). This predominantly brittle appearance on the fracture surface is in agreement with the tensile stress–strain curves shown in Fig. 7(a). For the UV-ZnO-1.5 nanocomposite shown in Fig. 11(b), the region of massive yielding has grown to substantially larger than that of UV-PP (shown in Fig. 11(a)). These yielding zones are located at the upper and lower part of the SEM micrograph in Fig. 11(b). As the nanoparticle content is increased to 5.0 wt%, the yielding zone (which is located at the upper and lower part of the SEM micrograph in Fig. 11(c)) has grown even larger, and occupies nearly 2/3 of the whole area of the fracture surface. This increase in yielding zone size with increasing ZnO nanoparticle content for the UV irradiation treated nanocomposites is consistent with the tensile test results (Fig. 7(a)) that the ductility increases with increasing nanoparticle content.

In order to better understand the effect of UV irradiation on the tensile fracture morphology, SEM examination has been focused on the tensile fracture surface region that is close to the specimen surface where UV damages are expected to be the most severe. Fig. 12(a) shows such damages for a UV-PP sample. It can be seen that severe cracks have been formed and propagated toward the interior of the specimen. These severe cracks are caused by the photo-degradation on the specimen surface. The presence of such cracks will definitely facilitate the failure under applied load. When examining the fracture surface for the UV-ZnO-3.0 nanocomposite, cracks can still be found (Fig. 12(b)), but the size of such sub-surface cracks has reduced dramatically (compare Fig. 12(a) and (b)). Under higher magnification SEM inspection, microcracks can be observed in both the UV-PP and UV-Zn-3.0 samples (Fig. 12(c) and (d)). These microcracks are highlighted by arrows in the respective SEM micrographs. It is clear that the number and size of the microcracks in UV-ZnO-3.0 (Fig. 12(d)) are less then those found in UV-PP (Fig. 12(c)).

3.6. Effect of UV irradiation on the thermal stability

The thermal stability and onset of degradation for polymers are usually improved by the incorporation of nanoparticles. Simultaneous DTA/TGA measurement results for PP, UV-PP, UV-ZnO-1.5, UV-ZnO-3.0, and UV-ZnO-5.0 are shown in Fig. 13. From the TGA and DTA curves, it is obvious that thermal decomposition for the different material systems are all one-step processes. In Fig. 13(a), it can be seen that the TGA curves for PP (before UV-irradiation treatment) and the UV-irradiated ZnO/PP nanocomposites are nearly overlapping each other. However, the thermal decomposition for UV-PP occurs at a significantly lower temperature and at a faster rate than the other systems. For the UV-irradiated ZnO/PP nanocomposites, due to the UV screening properties offered by the ZnO nanoparticles, the initiation of thermal decomposition temperature was raised. From the TGA curves in Fig. 13(a) the temperatures at 5% weight loss ($T_{-5\%}$) and maximum weight loss (T_{max}, which is defined at the peak of the derivative of the TGA curves) were measured and displayed in Table 3. From the $T_{-5\%}$ and T_{max} values, it can be found that the thermal stability for the ZnO/PP nanocomposites is better, because even after UV irradiation, the nanocomposites indicate higher $T_{-5\%}$ and T_{max} values. For the virgin PP after photo-degradation, the thermal stability drops dramatically. The superior thermal stability of photodegraded ZnO/PP nanocomposites is thus contributed to the protective effect of the ZnO nanoparticles upon UV irradiation. In the DTA curves shown in Fig. 13(b), the first peak around 185 °C corresponds to the melting of PP. The second peak is due to the thermal decomposition of PP, which shows a one-step decomposition mechanism. Thermal decomposition reactions start at above 300 °C through a radical chain reaction process. That is to say, carbon chain scission generates carbon centered radicals due to the lack of oxygen. These radicals then initiate and propagate the subsequent radical chain reactions [13].

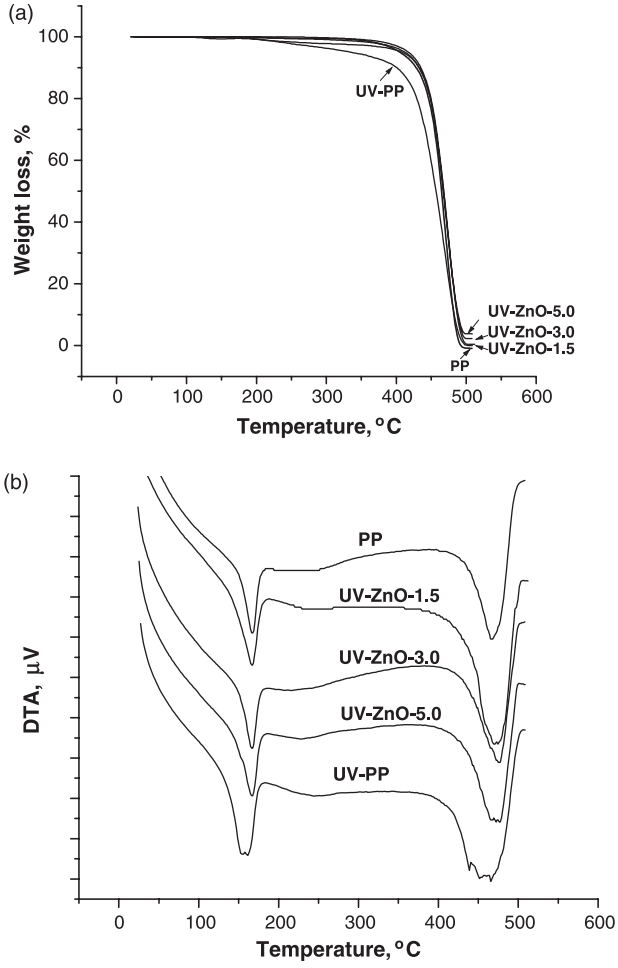

Fig. 13. Simultaneous TGA/DTA measurement results.

4. Conclusions

Results from this research study indicate that the incorporation of ZnO nanoparticles into PP matrix can impart significant improvements on the photo-degradation resistance of PP to UV-irradiation. From FTIR analysis centering the characteristic peaks around the carbonyl region (i.e. 1600–1800 cm^{-1}), it was observed that strong absorption bands were formed in the unfilled PP after subjected to UV-irradiation treatment. With the addition of ZnO nanoparticles into the PP matrix, the intensity of these carbonyl absorption bands was reduced in accordance with the increase in nanoparticle content.

Tensile test measurements indicated that the ZnO/PP nanocomposites remained ductile, with elongation at break (ε_b) values to be more than 500%, even with the incorporation of up to 5 wt% of ZnO nanoparticles. However, after the UV-irradiation treatment, ε_b for all the systems decreased dramatically. It is observed that ε_b for UV-PP was only 4%, and increased in a proportional manner to the increase in ZnO nanoparticle content. This indicates that the presence of ZnO nanoparticles in the nanocomposites can help to reduce the extent of photo-oxidation.

After UV-irradiation treatment, surface cracks were formed on the surface of all the investigated systems. Results from surface profile measurements supported that the surface cracking was more severe in unfilled PP, and the extent of surface cracking was found to reduce with increasing ZnO nanoparticle content. It is also found from SEM study that the size and density of the surface cracking is dramatically reduced in the ZnO/PP nanocomposites. In addition, TGA measurements on unfilled PP and the PP/ZnO nanocomposites show that, after UV irradiation, the ZnO/PP nanocomposites can maintain better thermal stability.

Acknowledgements

The work described in this paper was supported by a grant from the Research Grants Council of the Hong Kong Special Administrative Region, China (Project No. CityU 1202/02E).

References

[1] Allen NS, Edge M. Fundamentals of polymer degradation and stabilization. London: Elsevier Applied Science; 1992 [Chapter 4].
[2] Brambilla L, Consolati G, Gallo R, Quasso F, Severini F. Polymer 2003; 44:1041–4.
[3] Raab M, Kotulák L, Kolařík J, Pospíšil J. J Appl Polym Sci 1982;27: 2457–66.
[4] Kotek J, Kelnar I, Baldrian J, Raab M. Eur Polym J 2004;40:2731–8.
[5] Obadal M, Čermák R, Raab M, Verney V, Commereuc S, Fraïsse F. Polym Degrad Stab 2005;88:532–9.
[6] Shyichuk AV, Turton TJ, White JR, Syrotynska ID. Polym Degrad Stab 2004;86:377–83.
[7] Leong YW, Bakar MBA, Mohk Ishak ZA, Ariffin A. Polym Degrad Stab 2004;83:411–22.
[8] Rabello MS, White JR. Polymer 1997;38:6379–87.
[9] Allen NS, Chirinis-Padron A, Henman TJ. Polym Degrad Stab 1985;13: 31–76.
[10] Pandey JK, Reddy KR, Kumar AP, Singh RP. Polym Degrad Stab 2005; 88:234–50.
[11] Liufu SC, Xiao HN, Li YP. Polym Degrad Stab 2005;87:103–10.
[12] Zhu J, Morgan AB, Lamelas FJ, Wilkie CA. Chem Mater 2001;13: 3774–80.
[13] Zanetti M, Camino G, Reichert P, Mülhaupt R. Macromol Rapid Commun 2001;22:176–80.
[14] Qin H, Zhao C, Zhang S, Chen G, Yang M. Polym Degrad Stab 2003;81: 497–500.
[15] Qin H, Zhang S, Liu H, Xie S, Yang M, Shen D. Polymer 2005;46: 3149–56.
[16] Morlat S, Mailhot B, Gonzalez D, Gardette JL. Chem Mater 2004;16: 377–83.
[17] Tang Y, Hu Y, Song L, Zong R, Gui Z, Chen Z, et al. Polym Degrad Stab 2003;82:127–31.
[18] Maihot B, Morlat S, Gardette JL, Boucard S, Duchet J, Gérard JF. Polym Degrad Stab 2003;82:163–7.
[19] Yang R, Li Y, Yu J. Polym Degrad Stab 2005;88:168–74.
[20] White JR, Turnbull A. J Mater Sci 1994;29:584–613.
[21] Li R, Yabe S, Yamashita M, Momose S, Yoshida S, Yin S, et al. Mater Chem Phys 2002;75:39–44.
[22] Moustaghfir A, Tomasella E, Rivaton A, Mailhot B, Jacquet M, Gardette JL, et al. Surf Coat Technol 2004;180–181:642–5.
[23] Rabello MS, White JR. Polym Degrad Stab 1997;56:55–73.
[24] Brandrup J, Immergut EH. Polymer handbook, Part V. 3rd ed. New York: Wiley; 1989 p. 27.
[25] Jordana J, Jacobb KI, Tannenbaumc R, Sharafb MA, Jasiuk I. Mater Sci Eng 2005;393:1–11.
[26] Ash BJ, Siegel RW, Schadler LS. Macromolecules 2004;37:1358–69.
[27] Kaczmarek H, Oldak D, Malanowski P, Chaberska H. Polym Degrad Stab 2005;88:189–98.
[28] Marek A, Kaprálková L, Schmidt P, Pfleger J, Humlíček J, Pospíšil J, et al. Polym Degrad Stab 2006;91:444–58.
[29] Philippart JL, Sinturel C, Arnaud R, Gardette JL. Polym Degrad Stab 1999;64:213–25.
[30] Lacoste J, Vailiant D, Carlsson DJ. J Polym Sci 1993;31:715–22.
[31] Morlat S, Maihot B, Gonzalez D, Gardette JL. Chem Mater 2004;16: 377–83.
[32] Tang J, Wang Y, Liu H, Belfiore A. Polymer 2004;45:2081–91.
[33] Li Y, Wei GX, Sue HJ. J Mater Sci 2002;37:2447–59.
[34] Ma J, Zhang S, Qi Z, Li G, Hu Y. J Appl Polym Sci 2002;83:1978–85.
[35] Chan CM, Wu JS, Li JX, Cheung YK. Polymer 2002;43:2981–92.
[36] Karger-Kocsis J, editor. Polypropylene: structure, blends and composites. Structure and morphology, vol. 1. London: Chapman & Hall; 1995.
[37] Leung YH, Djurisic AB, Gao J, Xie MH, Wei ZF, Xu SJ, et al. Chem Phys Lett 2004;394:452–7.
[38] Zhao HX, Li RKY. J Polym Sci, Part B 2005;43:3652–64.
[39] Tjong SC, Shen JS, Li RKY. Polym Eng Sci 1996;36:100–5.
[40] Karger-Kocsis J, Mouzakis DE, Ehrenstein GW, Varga J. J Appl Polym Sci 1999;73:1205–14.
[41] Tjong SC, Shen JS, Li RKY. Polymer 1996;37:2309–16.
[42] Karger-Kocsis J, Varga J, Ehrenstein GW. J Appl Polym Sci 1997;64: 2057–66.
[43] Karger-Kocsis J, Varga J. J Appl Polym Sci 1996;62:291–300.